Analyst

Characterizing and Understanding the Photovoltage in n-Si/Au Light-Addressable Electrochemical Sensors

Journal:	*Analyst*
Manuscript ID	AN-COM-05-2024-000768.R1
Article Type:	Communication
Date Submitted by the Author:	11-Jun-2024
Complete List of Authors:	Hussain, Armeen; Montclair State University Mancini, Kayla; Montclair State University, Chemistry & Biochemistry Khatib, Yousef; Montclair State University O'Neil, Glen; Montclair State University, Chemistry; Montclair State University The Margaret and Herman Sokol Institute for Pharmaceutical Life Sciences

AN-COM-05-2024-000768– "Characterizing and Understanding the Photovoltage in n-Si/Au Light-Addressable Electrochemical Sensors" by Hussain, Mancini, Khatib, and O'Neil

Data Availability Statement

Data for this study, including EIS, AFM, and electrochemistry are available from the authors upon reasonable request.

COMMUNICATION

Characterizing and Understanding the Photovoltage in n-Si/Au Light-Addressable Electrochemical Sensors†

Armeen Hussain,[a,‡] Kayla Mancini,[a,‡] Yousef Khatib,[a] and Glen D. O'Neil*[a,b]

Received 00th January 20xx,
Accepted 00th January 20xx

DOI: 10.1039/x0xx00000x

Here, we characterize the photovoltage of n-Si/Au light-addressable electrodes (LAEs) over a range of solution potentials from ca. –1 to +1 V. We find that the n-Si/Au photoelectrodes show photovoltages consistent with a semiconductor/liquid junction in contrast to a buried junction, which opposes our previous understanding of how photovoltage originates in these sensors.

Light-addressable electrochemical (LAE) sensors are gaining significant attention because they enable a myriad of diverse applications in measurement science.[1,2] In an ideal scenario, the sensors are electrochemically inactive for a half-reaction (either oxidation or reduction) in the absence of illumination but become active when and where they are illuminated. While other methods exist for fabricating LAE sensors, we are particularly interested in LAE sensors based on semiconductor/metal (SM) or semiconductor/insulator/metal (MIS) junctions.[3–10] SM- and MIS-LAE sensors use a semiconductor to absorb light, separate electron/hole pairs (e^-/h^+), and transport e^-/h^+ to the appropriate interfaces, while the metal serves as the interface for the electrochemical reaction and depletes the semiconductor of minority carriers. SM and MIS junctions are also widely used for energy storage applications because sunlight can be used to drive the oxidation and reduction of water to O_2 and H_2, respectively.[11–14]

Photovoltage (V_{oc}) is the contra-thermodynamic shift in observed redox potential that occurs in depleted photoelectrodes and is an important parameter in photoelectrochemical (PEC) devices. In the context of PEC energy storage applications, V_{oc}, in conjunction with the short-circuit current density, determines the maximum output power, and therefore efficiency, of a device.[15] As a result, considerable research effort is dedicated to maximizing V_{oc}.[11–13,16]

In ideal SM junctions used for PEC where the metal layer is continuous and non-porous, V_{oc} is determined by the barrier height, i.e. the difference in Fermi level (E_f) of the semiconductor and metal.[17,18] However, these circumstances are rarely observed. For instance, Fermi-level pinning,[19] adaptive junctions,[18] and the pinch-off effect[20] can all lead to deviations from the ideal SM system. Another complication is that if the metal layer is very thin, then V_{oc} can be defined by the energy difference between the semiconductor and the redox species (i.e., a semiconductor/liquid junction)[21] due to inefficient screening by the metal. Therefore, SM interfaces for PEC are often complex and challenging to interpret, especially when they are heterogeneous (as is the case for the work presented here), leading to gaps in understanding, misinterpretations of experimental data, and hindering future development of measurement science techniques based on SM junctions.

In the context of LAE sensors, the impact of V_{oc} on sensor performance is less well-studied. For electroanalytical measurements, the position of the voltammetric peak is used to identify an analyte of interest. In electroanalytical measurements with metallic electrodes, the peak location is related to the standard reduction potential (E^0). However, for LAE, the peak position will be shifted from E^0 by the photovoltage. V_{oc} is cathodic for n-type semiconductors and anodic for p-type semiconductors. In the majority of early LAE sensor systems, a redox species was covalently bound to a semiconductor surface.[22,23] In these studies, V_{oc} arises from the difference between the semiconductor Fermi level and that of the redox species, similar to semiconductor/liquid junctions.[24] Under these circumstances, V_{oc} can only be changed by changing the redox species or semiconductor doping, or by creating a buried junction.[25] In contrast, Loget, Sojic and co-workers showed that the V_{oc} of MIS devices assembled using n-Si/SiOx/m junctions (where m=Pt, Ru, Ni, Co) for photo electrochemiluminescence (PECL) changed depending on the identity of the metal, suggesting a buried junction.[7–9] While these studies demonstrate that V_{oc} can be tuned for LAE sensors, they did not explore how changes in solution potential impact V_{oc}.

[a.] Department of Chemistry and Biochemistry, Montclair State University, Montclair, NJ, United States 07043
[b.] Sokol Institute for Pharmaceutical Life Sciences, Montclair State University, Montclair, NJ, United States 07043
‡ These authors contributed equally
†Electronic Supplementary Information (ESI) available: S1, Brief overview of semiconductor/metal and semiconductor/liquid junctions; S2, Experimental section, S3 Physical and Electrochemical Characterization of n-Si/Au photoelectrodes. See DOI: 10.1039/x0xx00000x

Here, we quantify V_{oc} on SM-LAE sensors using two distinct methods over a broad range of solution potentials (approximately –1 to + 1 V vs. SCE) at 85 mW cm^{-2} light intensity and explore the implications for LAE sensors. The intensity we used is sufficiently large for the response of the electrodes to be dictated by the electrochemistry, rather than the generation, transport, and collection of carriers.[26] First, we show that V_{oc} is dependent on the E_{sol} when the redox potential falls between the valence and conduction bands. However, when the redox potential is more positive than the valence band edge, V_{oc} is constant. Understanding the nature of V_{oc} on LAE sensors is important because the "effective" potential where analytes are expected for LAE sensors is a function of the formal potential ($E^{0'}$) and V_{oc}. A constant V_{oc} therefore should enable facile determination of an unknown molecule (or for a mixture of molecules).

We fabricated n-Si/Au and n-Si/Pt LAE sensors using electrodeposition as described in detail in the ESI Section 1. We characterized the sensors using a combination of x-ray photoelectron spectroscopy (XPS; Figure S2), atomic force microscopy (AFM; Figure S3), and electrochemical impedance spectroscopy (EIS; Figure S4) and cyclic voltammetry (CV; Figure S5) in aqueous ferrocene methanol (FcMeOH) solutions (ESI, Section S2). Elemental analysis with XPS shows that after electrodeposition, the n-Si is coated with a discontinuous layer of Au. AFM showed that the surfaces were covered with a discontinuous metal film composed of small (~50 nm) nanoparticles. EIS was used to determine the flat band potential (E_{fb}) to be approximately –0.68(±0.02) V vs. SCE by determining the inverse square capacitance as a function of applied potential (i.e., the Mott-Schottky method).[27] Note that pH was not rigorously controlled in these measurements (see ESI, Section S2). From the plots of C^{-2} vs. E we were also able to estimate the positions of the valence band (E_v) and conduction band edges (E_c) to be 0.17(±0.02) and –0.93(±0.02) V vs. SCE, respectively. CV in FcMeOH showed that the samples had near-reversible electrochemistry under illumination, consistent with fast charge transfer (both within the Si and across the interfaces), and near-zero anodic dark currents. These data are consistent with our previous results.[3,4]

Figure 1 shows schematic energy band diagrams of the semiconductor (sc), metal (m), and redox species (O/R). The semiconductor is characterized by E_v, E_c, and electron Fermi level ($E_{f,n}$). The metal is characterized by its Fermi level ($E_{f,m}$). The redox species is characterized by its standard reduction potential (E^0). The E_f of the two solid phases and the E^0 of the redox species are all related to the electrochemical potential of electrons in their respective phases.[28] At equilibrium in the dark, the electrochemical potentials of all three phases equilibrate (Figure 1b). Therefore a measurement of the cell potential in the dark should inform how the energy bands align at equilibrium. When the semiconductor is illuminated with light having more energy than the band gap energy (E_g), e^-/h^+ are generated in the valence band, e^- are excited to the conduction band, and the holes are transferred to the sc/m interface. The generation of e^-/h^+ changes the population of electrons in the valence and conduction bands, which in turn shifts the fermi level towards more anodic potentials ($E_{f,p}$). This shift in fermi level is the origin of photovoltage (Figure 1c).

We performed square wave voltammetry (SWV) to illustrate the effect of V_{oc} on voltammetric measurements over a broad potential range. Figure 2 shows a series of representative SWVs

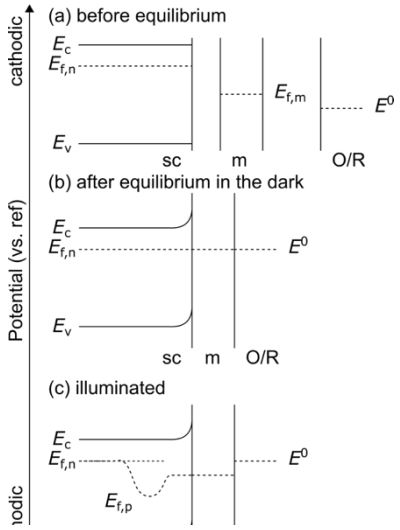

Figure 1. Schematic band diagrams showing the relative alignment of energy for semiconductor, metal, and redox species: (a) under pre-equilibrium conditions, (b) at equilibrium in the dark, and (c) under illumination. Note that these diagrams are not to scale.

for the oxidation of (a) tris(bipyridine)ruthenium(II) ($Ru(bpy)_3^{3+}$), (b) hexachloroiridate(IV) ($IrCl_6^{2-}$), (c) ferrocene methanol (FcMeOH), and the reduction of (d) hexaammineruthenium(III) ($Ru(NH_3)_6^{3+}$) and (e) methyl viologen (MV^{2+}) on n-Si/Au LAE in the light (red traces) and dark (black traces). Also displayed in Figure 2 are control measurements prepared with highly doped p^+-Si/Au electrodes (blue traces). These redox species were chosen because they: (i) have a broad range of redox potentials ($-1.01 \leq E^{0'} \leq 1.05$ V vs. SCE), (ii) have fast heterogeneous electron transfer kinetics on the n-Si/Au and p^+-Si/Au electrodes. We used SWV to probe the photoelectrochemistry because both oxidation and reduction reactions are light-addressable when using SWV.[4]

The SWVs in Figure 2a-e show that the voltammetry is well-behaved over a very broad potential range (ca. ±1 V vs. SCE) for samples prepared with both n-Si and p^+Si. For $Ru(bpy)_3^{3+}$, $IrCl_6^{2-}$, FcMeOH, and $Ru(NH)_6^{3+}$ a single redox wave is observed under illumination (note that the SWV presents a differential current measurement and all currents are presented as positive). However, for MV^{2+} there are two reductions observed within the scan window. The first reduction ($E_{1/2} \approx -0.66$ V) shows a single peak while the second reduction ($E_{1/2} \approx -1$ V) shows split peaks, consistent with slow electron transfer kinetics. We estimated V_{oc} for each redox species by measuring the difference in peak potential (Ep) for a given redox species using the n-Si/Au and p^+-Si/Au samples (i.e., the blue and red traces in Figure 2). Figure 2f shows V_{oc} as a function of the $E_{1/2}$ value of the redox species, as determined using the peak location of the p^+Si/Au sensors. Over the range from ≈–1 to ≈0.2 V the change in V_{oc} is linear ($R^2 = 0.999$), while V_{oc} is constant when $E_{1/2} > 0$ V vs. SCE.

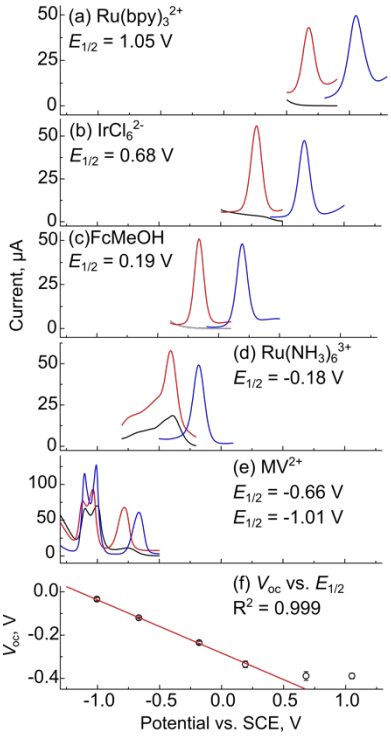

Figure 2. SW voltammograms that were collected using n-Si/Au (red and black traces) and p⁺Si/Au (blue traces) in aqueous electrolytes containing 0.1 M KNO_3 and 1 mM (a) $Ru(bpy)_3^{3+}$, (b) $IrCl_6^{2-}$, (c) FcMeOH, (d) $Ru(NH_3)_6^{3+}$, and (e) MV^{2+}. SWV parameters were E_{step} = 4 mV, E_{amp} = 25 mV, f = 25 Hz. (f) Plot of V_{oc} versus $E_{1/2}$ for the redox species tested in parts (a)-(e). Symbols represent the mean of 3 separately prepared samples and error bars represent one standard deviation.

We performed chopped light open circuit potential (OCP; i.e., E_{cell}) measurements to understand how the band energetics change in the dark and under illumination. Figure 3a shows a chopped light OCP trace for a solution of 5 mM $Fe(CN)_6^{4-}$ and 5 mM $Fe(CN)_6^{3-}$. The green bars in Figure 3a indicate when the photoelectrode was illuminated with 85 mW cm^{-2} white light. When the illumination condition changes from light to dark, the potential rapidly stabilizes, due in part to the fast charge transfer at the interfaces and the fast electron transfer with the redox mediator. Under illumination, E_{cell} is considerably more negative than in the dark because of V_{oc}. To determine if the E_{cell} changed with E_{sol}, we prepared a variety of solutions with E_{sol} ranging from 0.04 to 0.78 V vs. Ag/AgCl. We prepared these solutions using two redox species with fast electron transfer kinetics: $Fe(CN)_6^{4-/3-}$ (circles) and $IrCl_6^{3-/2-}$ (squares). The solution potential was varied by changing the concentration ratio of oxidized and reduced species according to the Nernst Equation:

$$E_{sol} = E^0 + {}^{RT}/_{nF} \ln\left(A_{ox}/A_{red}\right) \quad (1)$$

where E_{sol} is the solution potential, E^0 is the formal potential of the redox couple, R is the ideal gas constant, T is the absolute temperature, n is the number of electrons transferred in the redox reaction, F is Faraday's constant, and A is the activity of the redox species. E_{sol} was measured for each solution using a polished 2 mm gold disk electrode. These data were acquired using 6 independently prepared samples.

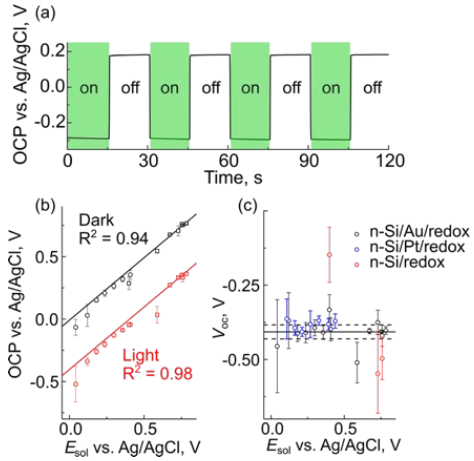

Figure 3. (a) Chopped-light OCP measurements acquired using an n-Si/Au LAE sensor in an electrolyte containing 5 mM $Fe(CN)_6^{4-}$, 5 mM $Fe(CN)_6^{3-}$, and 0.1 M KNO_3. Light was 85 mW cm^{-2} white light. (b) Measured OCP as a function of E_{sol} for n-Si/Au sensors in the dark (black data) and under illumination (red data). Solution potential was varied by changing the concentrations of two redox couples: $Fe(CN)_6^{4-/3-}$ (circles) and $IrCl_6^{3-/2-}$ (squares). (c) V_{oc} versus E_{sol} for n-Si/Au, n-Si/Pt, and freshly etched n-Si. Symbols in parts (b) and (c) are the mean of 3 separately prepared samples. Error bars in (b) represent the standard deviation of three separate trials. Error bars in (c) are propagated from the standard deviations in part (b).

The black trace in Fig 3b shows that the cell potential varies linearly (m≈1; R^2=0.94) with the solution potential in the dark, demonstrating that the semiconductor and metal are equilibrated with E_{sol} in the dark. When the semiconductor is illuminated, electron-hole pairs (e^-/h^+) form, are separated by the electric field within the semiconductor, and are transported to the appropriate interfaces (holes to the sensing interface and electrons to the Ohmic back contact). The increase in holes near the interface causes the Fermi level of the semiconductor to split (Figure 1c), leading to V_{oc}. The red trace in Figure 3b shows E_{cell} as a function of E_{sol} from 0.04 to 0.78 V vs. Ag/AgCl under illumination. Similar to the black trace in Figure 3b, the two potentials are strongly correlated (m≈1; R^2=0.98).

V_{oc} is calculated from the difference in E_{cell} in the dark and under illumination ($V_{oc} = E_{cell,light} - E_{cell,dark}$). The black circles in Figure 3c show V_{oc} as a function of E_{sol} for an n-Si/Au LAE sensor. The data show a consistent V_{oc} over the measured potential range. The solid black line in Figure 3c represents the mean V_{oc} of the pooled data (= –0.41 V) and the dotted lines represent the 95% confidence intervals (= ±0.02 V) for the pooled data. These data agree very well with the V_{oc} data measured independently using SWV (Figure 2).

As a control experiment, we measured the OCP using freshly etched n-Si electrodes in direct contact with the $IrCl_6^{3-/2-}$ redox couple in the dark and under illumination. The samples were freshly etched before each 60 s OCP measurement to minimize the impact of the passivating SiOx species. The V_{oc} for these samples (red dots in Figure 3c) changes with the solution potential, becoming smaller with decreasing E_{sol}. This behavior is consistent with unpinned semiconductor/liquid contacts.[21,29]

We prepared n-Si/Pt LAE sensors similar to our previous report[5] and measured the V_{oc} for these samples using the OCP method in $Fe(CN)_6^{4-/3-}$ solutions (blue circles in Figure 3c). We hypothesized that if the SM junction was responsible for V_{oc}

generation (and the junction was not Fermi-level pinned), a significant difference in V_{oc} would be observed due to differences in the work functions of Au and Pt (≈5.3 and 5.6 eV, respectively) leading to different barrier heights and photovoltages. Over the range of E_{sol} studied n-Si/Pt LAE sensors had nearly identical V_{oc} values compared with n-Si/Au sensors. These data suggest that the semiconductor/metal interface is not the photovoltage-generating interface. An alternative interpretation is that these sensors are experiencing Fermi-level pinning;[20,30] however, this interpretation is not consistent with the data in Figure 2, which shows that V_{oc} changes linearly with E^0 when E^0 is between the valence and conduction bands.

The results in Figures 2 and 3 suggest the following mechanism for V_{oc} generation for electrodeposited semiconductor/metal LAE sensors. When E_{sol} is between the valence and conduction band edges, V_{oc} changes linearly with E_{sol}. We observe that when E_{sol} is close in energy to E_{cb} then V_{oc} is close to 0 mV, but as E_{sol} approaches the E_{vb} then V_{oc} approaches 0.4 V (Figure 2f). When E_{sol} is more positive than E_{vb}, V_{oc} is mostly stable at ≈0.4 V (Figure 3c). Importantly, the values of V_{oc} were determined by two separate methods and are consistent with one another (Figure S6). These data strongly suggest that V_{oc} is determined by the difference in electrochemical potential between the redox species and the semiconductor. We suggest that the Fermi level of the Au equilibrates with the redox species in solution, thereby tuning the Au Fermi level with changes in E^0. This may be caused by the thin Au layer prepared via electrodeposition and has been proposed for thin Ni layers on n-Si.[31]

These data are significant because when using electrochemical sensors, the redox potential is often used to determine the identity of a reacting species. When using LAE sensors, the observed effective potential differs from the thermodynamic value by V_{oc}, and so understanding the origin of that shift is critical for the future development of new LAE sensors. The results presented show that V_{oc} is effectively constant over a ≈1 V range when $E_{sol} > 0$ V vs. SCE. Interestingly, constant V_{oc} levels are not desirable for PEC water-splitting applications but are very adventitious for LAE sensors. More generally, it also demonstrates the importance of characterizing the photovoltage over a broad range of potentials and the necessity to determine the band energetics for n-Si/m LAE sensors.

We acknowledge support from the Research Corporation for Science Advancement for a Cottrell Scholars Award, a CAREER award from the National Science Foundation (CBET-1944432), and the National Science Foundation Major Research Instrumentation Program (CHE-2215861). We thank Dr. Xu Feng at the Surface Analysis Facility at the University of Delaware for XPS measurements. The XPS was supported by a grant from the National Science Foundation Major Research Instrumentation Program (CHE-1428149).

Author Contributions

AH performed all open circuit potential measurements and analyzed the data. KM and YK performed all SWV and EIS measurements and analyzed the data. KM prepared samples for XPS and performed AFM measurements. GDO performed experimental design, project management, data analysis, writing (first draft and editing), and funding acquisition.

Conflicts of interest

The authors declare no conflicts of interest.

1 Y. B. Vogel, J. J. Gooding and S. Ciampi, *Chem. Soc. Rev.*, 2019, **48**, 3723–3739.
2 Y. Meng, F. Chen, C. Wu, J. Wang and D. Zhang, *ACS Sensors*, 2022, **7**, 1791–1807.
3 I. M. Terrero Rodríguez, A. J. Borrill, K. J. Schaffer, J. B. Hernandez and G. D. O'Neil, *Anal. Chem.*, 2020, **92**, 11444–11452.
4 E. G. Arthur, H. Ali, A. Hussain and G. D. O'Neil, *Anal. Chem.*, 2023, **95**, 9219–9226.
5 J. B. Hernandez, Z. B. Epright, I. M. Terrero Rodríguez and G. D. O'Neil, *ChemElectroChem*, , DOI:10.1002/celc.202300400.
6 Y. Zhao, J. Yu, G. Xu, N. Sojic and G. Loget, *Journal of the American Chemical Society*, 2019, **141**, 13013–13016.
7 Y. Zhao, J. Descamps, S. Ababou-Girard, J.-F. Bergamini, L. Santinacci, Y. Léger, N. Sojic and G. Loget, *Angewandte Chemie International Edition*, 2022, **61**, e202201865.
8 Y. Zhao, L. Bouffier, G. Xu, G. Loget and N. Sojic, *Chemical Science*, 2022, **2022**, 2528–2550.
9 Y. Zhao, J. Descamps, N. Al Hoda Al Bast, M. Duque, J. Esteve, B. Sepulveda, G. Loget and N. Sojic, *J. Am. Chem. Soc.*, 2023, jacs.3c05856.
10 H. Li, W. Hao, J. Hu and H. Wu, *Biosensors and Bioelectronics*, 2013, **47**, 225–230.
11 A. G. Scheuermann, J. P. Lawrence, K. W. Kemp, T. Ito, A. Walsh, C. E. D. Chidsey, P. K. Hurley and P. C. McIntyre, *Nature Materials*, 2016, **15**, 99–105.
12 I. A. Digdaya, G. W. P. Adhyaksa, B. J. Trześniewski, E. C. Garnett and W. A. Smith, *Nature Communications*, 2017, **8**, 15938.
13 I. A. Digdaya, B. J. Trześniewski, G. W. P. Adhyaksa, E. C. Garnett and W. A. Smith, *Journal of Physical Chemistry C*, 2018, **122**, 5462–5471.
14 Q. Chen and J. A. Switzer, *ACS Applied Materials and Interfaces*, 2018, **10**, 21365–21371.
15 M. G. Walter, E. L. Warren, J. R. McKone, S. W. Boettcher, Q. Mi, E. A. Santori and N. S. Lewis, *Chem. Rev.*, 2010, **110**, 6446–6473.
16 W. A. Smith, I. D. Sharp, N. C. Strandwitz and J. Bisquert, *Energy Environ. Sci.*, 2015, **8**, 2851–2862.
17 T. J. Mills, F. Lin and S. W. Boettcher, *Physical Review Letters*, , DOI:10.1103/PhysRevLett.112.148304.
18 M. R. Nellist, F. A. L. Laskowski, F. Lin, T. J. Mills and S. W. Boettcher, *Accounts of Chemical Research*, 2016, **49**, 733–740.
19 F.-R. F. Fan, T. V. Shea and A. J. Bard, .
20 R. T. Tung, *Applied Physics Reviews*, , DOI:10.1063/1.4858400.
21 A. Kumar, W. C. A. Wilisch and N. S. Lewis, *Critical Reviews in Solid State and Materials Sciences*, 1993, **18**, 327–353.
22 M. H. Choudhury, S. Ciampi, Y. Yang, R. Tavallaie, Y. Zhu, L. Zarei, V. R. Gonçales and J. J. Gooding, *Chem. Sci.*, 2015, **6**, 6769–6776.
23 Y. Yang, M. Cuartero, V. R. Gonåales, J. J. Gooding, E. Bakker, V. R. Gonçales, J. J. Gooding and E. Bakker, *Angewandte Chemie International Edition*, 2018, **57**, 16801–16805.
24 J. Gobrecht and H. Gerischer, *Solar Energy Materials*, 1979, **2**, 131–142.
25 V. R. Gonçales, J. Lian, S. Gautam, D. Hagness, Y. Yang, R. D. Tilley, S. Ciampi and J. J. Gooding, *Journal of Physical Chemistry C*, 2020, **124**, 836–844.
26 J. T. Davis and D. V. Esposito, *Journal of Physics D: Applied Physics*, 2017, **50**, 084002.
27 K. Gelderman, L. Lee and S. W. Donne, *Journal of Chemical Education*, 2007, **84**, 685.

28 S. W. Boettcher, S. Z. Oener, M. C. Lonergan, Y. Surendranath, S. Ardo, C. Brozek and P. A. Kempler, *ACS Energy Letters*, 2021, **6**, 261–266.
29 P. Nunez, M. Cabán-Acevedo, W. Yu, M. H. Richter, K. Kennedy, A. M. Villarino, B. S. Brunschwig and N. S. Lewis, *J. Phys. Chem. C*, 2021, **125**, 17660–17670.
30 S. M. Sze and K. K. Ng, *Physics of semiconductor devices*, Wiley-Interscience, Hoboken, N.J, 3rd ed., 2007.
31 M. J. Kenney, M. Gong, Y. Li, J. Z. Wu, J. Feng, M. Lanza and H. Dai, *Science*, 2013, **342**, 836–840.